Materials Today Bio 31 (2025) 101515

Contents lists available at ScienceDirect

Materials Today Bio

journal homepage: www.journals.elsevier.com/materials-today-bio

3D bioprinting lobule-like hepatorganoids with induced vascularization for orthotopic implantation

Jianing Yan [a,b,c,1], Zhichao Ye [a,b,c,1], Yiwei Lu [a,b,c,1], Yuyang Yuan [a,b,c], Xiaofeng Wang [d], Tingting Yan [a,b,c], Jun Yin [e,f,**], Yifan Wang [a,b,c,*]

[a] Department of General Surgery, Sir Run Run Shaw Hospital Affiliated to School of Medicine, Zhejiang University, Hangzhou, 310016, China
[b] National Engineering Research Center of Innovation and Application of Minimally Invasive Instruments, Hangzhou, 310016, China
[c] Zhejiang Provincial Key Laboratory of Laparoscopic Technology, Sir Run Run Shaw Hospital Affiliated to School of Medicine, Zhejiang University, Hangzhou, 310016, China
[d] Department of Plastic Surgery, Sir Run Run Shaw Hospital Affiliated to School of Medicine, Zhejiang University, Hangzhou, 310016, China
[e] The State Key Laboratory of Fluid Power and Mechatronic Systems, School of Mechanical Engineering, Zhejiang University, Hangzhou, 310028, China
[f] Key Laboratory of 3D Printing Process and Equipment of Zhejiang Province, School of Mechanical Engineering, Zhejiang University, Hangzhou, 310028, China

A B S T R A C T

Orthotopic implantation *in vivo* is the ultimate target of tissue-engineering organoids research, aiming to achieve sustaining survival after implantation. However, the limited representation of a complex microenvironment in implanted accepter hampers a comprehensive understanding of long-term maintenance of tissue-engineering organoids, especially in liver. In this research, we developed a 3D bioprinting method using gelatin methacryloyl (GelMA) hydrogel to fabricate lobule-like hepatorganoids, which faithfully mimic the structure of hepatic lobules with lower level of hypoxia (lobule vs 60°, 90°, control; 0.4880 vs 1.009, 0.6778, 0.8704; $p < 0.01$), high secretion of albumin (lobule vs 60°, 90°, control; 13.47 vs 12.39, 12.65, 10.08 mg/L; $p < 0.01$) and urea (lobule vs 60°, 90°, control; 5.304 vs 5.233, 4.781, 4.358 mg/L; $p < 0.01$) in vitro; and promotion of angiogenesis and maintenance of activity following orthotopic implantation. Loaded with a prolonged released system of vascular endothelial growth factor (VEGF) and infused with human umbilical vein endothelial cells (HUVECs), we developed a fabricating method of vascularized lobule-like hepatorganoids (VLH) which possessed promoted vascularization. We identified GAS6/AXL and LAMB3/ITGA3 signaling pathway up-regulated in VLH, which was conducive to vascularization and proliferation. Furthermore, orthotopic implantation model indicated that VLH exhibited prolonged survival *in vivo*, with elevated level of serological biomarkers and more abundant vascularization in grafts. Eventually, our findings demonstrate that this system effectively forms orthotopic implantation of hepatorganoids and facilitates vascularization, which may notably contribute to the understanding of transplantation, drug screening, and replacement therapy.

1. Introduction

Liver is the central organ of physiological activities in body, encompassing more than 500 synthetic and metabolic functions [1,2]. Liver transplantation is currently the most effective treatment for end-stage hepatic disorder in clinical practice. However, the availability of donor remains a remarkable limiting factor for liver transplantation. Hepatorganoids holds the potential to overcome the current bottleneck in hepatic provision, with combining the advantages while overcoming the drawbacks of both liver transplantation [3]. Recent studies have reported that implanting tissue engineering hepatorganoids into animal models of liver failure significantly prolongs the survival, showing promising therapeutic effects for liver dysfunction [4,5]. Meanwhile, through bio-manufacturing techniques, tissue engineering hepatorganoids can be fabricated in a standardized and industrialized procedure, leading to reduced production costs.

The establishment of vascularization in tissue engineering hepatorganoids is of utmost importance for long-term cultivation, maintenance of the cellular microenvironment and preservation of survival [6]. Several advanced tissue engineering manufacturing methods aimed to

* Corresponding author. Department of General Surgery, Sir Run Run Shaw Hospital Affiliated to School of Medicine, Zhejiang University, Hangzhou, 310016, China.
** Corresponding author. The State Key Laboratory of Fluid Power and Mechatronic Systems, School of Mechanical Engineering, Zhejiang University, Hangzhou, 310028, China.
E-mail addresses: junyin@zju.edu.cn (J. Yin), anwyf@zju.edu.cn (Y. Wang).
[1] These authors contribute equally.

https://doi.org/10.1016/j.mtbio.2025.101515
Received 25 September 2024; Received in revised form 15 January 2025; Accepted 20 January 2025
Available online 22 January 2025

create biomimetic liver microtissues with structural and functional similarities to the native liver lobule [6–11]. In particular, emerging 3D bioprinting technology enables high-precision fabrication of complex architectures and patterns, facilitating cell-matrix interactions and vascularization. Currently, most researches primarily focus on in vitro studies, including optimization of biomaterials and process, development of liver disease models for drug screening, and *in vivo* studies though subcutaneous implantation. However, there remains insufficient researches concerning the orthotopic implantation and dynamic monitoring of activity within the liver.

The long-term controlled release of vascular endothelial growth factor (VEGF) also plays a crucial role in vascularization and tissue engineering. VEGF is a potent angiogenic cytokine that stimulates the growth of new blood vessels from pre-existing vasculature. The dose of VEGF can control the coupling of angiogenesis and other tissue growth [12]. Studies have shown that VEGF loaded into biomaterials can enhance 3D endothelial cell migration and vascularization. VEGF incorporated into heparinized hyaluronic acid macroporous hydrogels, which improve endothelial cell migration and vascularization [13]. VEGF-decorated extracellular matrices can effectively improve vascular invasion for coupling of angiogenesis and osteogenesis [14]. VEGF encapsulated in spray-dried alginate microparticles within collagen-hydroxyapatite scaffolds can promote vascularization and bone repair by providing a sustained release of the growth factor [15].

Here, we integrate an N-hydroxysuccinimide (NHS) modified dual-functional polyethylene glycol (PEG) cross-linker (AC-PEG-NHS) to load vascular endothelial growth factor (VEGF) and construct a VEGF-controlled-releasing methacrylate gelatin (GelMA) hydrogel (GelMA/NHS/VEGF), facilitating the spontaneous self-assembly of human umbilical vein endothelial cells (HUVECs) to form capillary networks. Consequently, utilizing technology of tissue engineering, we develop a 3D bioprinting lobule-like hepatorganoids with induced vascularization, which possesses promotion of angiogenesis and maintenance of activity and functionality following orthotopic implantation. Through RNA sequencing, we identify GAS6/AXL and LAMB3/ITGA3 signaling pathway up-regulated in vascularized lobule-like hepatorganoids, which remarkably contribute to angiogenesis and proliferation (Fig. 1).

2. Methods

2.1. Materials

N-hydroxysuccinimide modified dual-functional polyethylene glycol cross-linker (AC-PEG-NHS), methacrylate gelatin (GelMA) and lithium phenyl(2,4,6-trimethylbenzoyl) phosphinate (LAP) were purchased from Engineering For Life (Cat. No. EFL-AC-PEG-NHS; EFL-GM-60, EFL-LAP). Murine vascular endothelial growth factor (VEGF) was purchased from Peprotech (Cat. No. 450-32). Matrigel was purchased from Corning (Cat. No. 356234).

For RT-qPCR, RNA purification kits were procured from Esunbio (RN001 China). The strand cDNA synthesis and qPCR SYBR Green Master Mix kit was acquired from Yeasen Biotech. (HB200729 China). RT-qPCR primers were designed using the PrimerBank website (https://pga.mgh.harvard. edu/primerbank/) and were blasted through the NCBI Basic Local Alignment Search Tool website (https://blast.ncbi.nlm.nih.gov/Blast.cgi). Primer sequences for RT-qPCR: GAS6-F: 5′-CTCGTGCAGCCTATAAACCCT-3’; GAS6-R: 5′- TCCTCGTGTTCACTTTCACCG-3’; AXL-F: 5′- ATCAGCTTCGGCTAGGCAG-3’; AXL-R: 5′-TCCGCGTAGCACTAATGTTCT-3’; LAMB3-F: 5′-GCAGCCTCACAACTACTACAG-3’; LAMB3-R: 5′- CCAGGTCTTACCGAAGTCTGA-3’; ITGA3-F: 5′-TCAACCTGGATACCCGATTCC-3’; ITGA3-R: 5′- GCTCTGTCTGCCGATGGAG-3’; GAPDH-F: 5′-TCGACAGTCAGCCGCATCTTCTTT-3’; GAPDH-R: 5′-ACCAAATCCGTTGACTCCGACCTT-3’.

For immunofluorescence, primary antibody anti-ALB and anti-AXL were purchased from Abclonal (Cat. No. A24161, A17874, China). Anti-MRP2 was purchased from Abcam (Cat. No. ab172630, USA). Anti-GAS6, anti-ITGA3 and anti-LAMB3 were purchased from Proteintech (Cat. No. 13795-1-AP, 66070-1-Ig, 26795-1-AP, China). ABflo488-conjugated and ABflo594-conjugated secondary antibody were purchased from Abclonal (Cat. No. AS053 and AS054, China). For

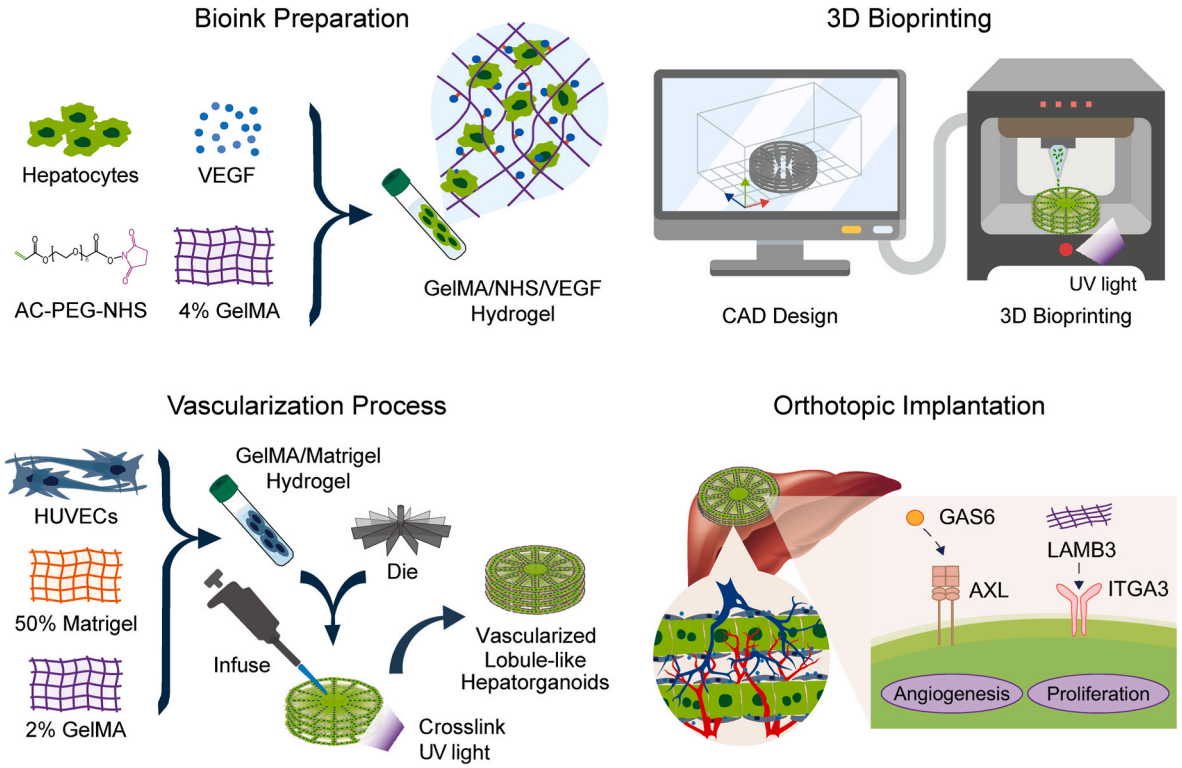

Fig. 1. Scheme diagram of manufacturing 3D bioprinting vascularized lobule-like hepatorganoids for orthotopic implantation.

immunohistochemistry, anti-hCD31 from a primary antibodies panel and 2-step plus® Poly-HRP Anti-Mouse/Rabbit IgG EnVision Detection System were purchased from ZSGB-BIO Inc. (PV9000, China). Anti-mCD31 was purchased from Abcam (Cat. No. ab9498, USA)

Mouse VEGFA ELISA kit and human albumin ELISA kit were purchased from Abclonal (Cat. No. RK0028, RK00157). Urea nitrogen assay kit was purchased from Sangon Biotech (Cat. D799850). Calcein-AM/PI live/dead assay kit was purchased from Beyotime (Cat. No. C2015S). Image-iT™ Green Hypoxia Reagent was purchased from Thermo Fisher (Cat. No. I14834). For live imaging, D-luciferin potassium salt was purchased from Beyotime (Cat. No. ST198). Cy5.5 was purchased from MedChemExpress (Cat. No. 210892-23-2).

2.2. Cell culture and luciferase expressing-cell construction

Human umbilical vascular endothelial cell (HUVEC), immortalized mouse cell line AML12, human hepatic cell line Huh7 and 293T cells were procured from Chinese Academy of Sciences. Cells were maintained in DMEM culture medium (Thermo Fisher, USA), supplemented with 10 % fetal bovine serum (Thermo Fisher, USA) and 1 % penicillin/streptomycin (Beyotime, China). The cells were cultured in 37 °C incubators with 5 % CO_2. When reaching 80 % confluence, cells were digested by 0.05 % trypsin (Beyotime, China) and passaged.

To establish a co-culture system for Huh7 and HUVECs. We seed Huh7 cells into the lower chamber and HUVECs onto the upper surface of Transwell inserts. DMEM supplemented with 10 % fetal bovine serum and 1 % penicillin/streptomycin was used as the culture medium for co-culturing. Maintain the co-culture at 37 °C with 5 % CO2, changing the medium every 1–2 days. This setup allows for the study of interactions between Huh7 and HUVECs in a controlled environment.

For lentivirus construction, expressing vector (pBOBi-luc-IRES-GFP) and packaging vectors (pVSVG, pMDL and pRSV-Rev) were co-transfected into 293T cells at a ratio of 3:1:1:1. Following lentivirus collection, Huh7 cells were infected by pBOBi-luc-IRES-GFP lentivirus and subsequently sorted using flow cytometry.

2.3. Synthesis of GelMA/NHS/VEGF

For synthesis of GelMA/NHS/VEGF, AC-PEG-NHS (30 mg/mL) was added into VEGF solution (0.5 g/mL). After filtrating by sterile filter, the composite solution was incubated in 4 °C overnight. Subsequently, the AC-PEG-NHS-VEGF solution was mixed with 4 % GelMA solution and photocured under UV light to synthesis GelMA/NHS/VEGF hydrogel.

2.4. Materials characterization and scanning electron microscope (SEM)

The mechanical properties of the hydrogels were assessed using a commercial tensile machine (ElectroForce Testbench, TA Instruments, USA). Uniaxial tensile tests were conducted at room temperature with a deflection speed of 1 mm/min. The samples were secured between two test clamps initially set apart by 3.5 mm. Stress-strain curves were documented during testing, and Young's modulus was calculated as the slope of the stress-strain curve by linear fitting within the range between 0 and 10 % strain. Each group underwent testing with a minimum of 3 specimens.

For scanning electron microscopy (SEM), the images and elemental analysis were obtained using a thermal field emission scanning electron microscope (GEMINI 300, ZEISS).

2.5. Calcein-AM/PI live/dead assay and Image-iT™ green hypoxia assay

Calcein-AM and PI were diluted at a ratio of 1:1000 with buffer. Subsequently, the samples were incubated with the Calcein-AM/PI solution at 37 °C for 20mins and observed under a fluorescence microscope (EVOS Cell Imaging Systems, Thermo Fisher Scientific, USA).

For detecting hypoxia condition in hepatorganoids, the Image-iT™ green reagent was added into the appropriate cell medium at 5 μM. The hepatorganoids were incubated at 37 °C for 1 h and observed under a fluorescence microscope.

2.6. VEGF-releasing test

After the preparation of GelMA/NHS/VEGF accomplished, the hydrogels were immerged in medium at 37 °C. The medium was collected on day 0, day 1, day 2, day 4, day 7 and day 14, for VEGF level measurement through ELISA as per following protocol.

2.7. Enzyme-lineked immunosorbent assay (ELISA) and urea nitrogen assay

Samples and antigen-specific antibodies were added into wells on coated microplates. Then, the microplates were incubated at 37 °C for 1 h and washed by washing buffer for at least 5 times to remove unbound antigens and antibodies. Then, the enzyme-linked detection antibodies were added into wells to bind to captured antibodies. After incubated at 37 °C for 1 h, the microplates were washed by washing buffer for at least 5 times to remove unbound detection antibodies. Then, substrates for the enzyme were added into wells leading to color changes, and the reaction was stopped using acid. The color intensity was measured by a spectrophotometer (Multiskan GO, Thermo Scientific, USA).

For urea nitrogen assay, samples were collected and processed with the reagents according to the protocol of urea nitrogen assay kit, micromethod. The spectrophotometer was used to measure the color intensity.

2.8. Degradation in vivo

For validating degradation of hydrogels *in vivo,* GelMA/NHS/VEGF and 4 % GelMA hydrogels were shaped to cylinder by mold (0.5 cm in diameter and 0.1 cm in depth). After stained by Cy5.5 solution (10 μM), GelMA/NHS/VEGF and 4 % GelMA hydrogels were separately implanted subcutaneously on left and right side back of nude mice. The signal of Cy5.5 was detected on different time points to indicate degradation of hydrogels *in vivo*.

2.9. Live imaging

The live imaging was conducted with PerkinElmer imaging system from Caliper Life Sciences, USA. After anesthesia, the animal was secured on the imaging platform for stability. For bioluminescence imaging, the signal of Cy5.5 was directly detected and quantified. For fluorescence imaging, an intraperitoneal injection of D-luciferin potassium salt solution (15 mg/mL) in a volume of approximately 10 μl/g was administered, and the animal was detected after 10–20mins post-injection.

2.10. 3D bioprinting

A 3D cell printer (Envision TEC 3D Bioplotter) was employed to fabricate in vitro liver constructs. The cells were first harvested and prepared for suspension. Cell counting was performed using a hemocytometer to ensure an accurate cell density. A small volume of cell suspension was mixed with trypan blue dye to distinguish viable cells from non-viable ones. The mixture was then loaded onto Countess™ 3 FL Automated Cell Counter. Based on the counted cell number, the cell suspension was adjusted to achieve a final cell density of 2×10^7/mL. For huh7 cells and 293T cells, the cell suspension was mixed with an 8 % GelMA solution at a 1:1 vol ratio (v/v). For HUVEC cells, the cell suspension was mixed with an 4 % GelMA/50 % Matrigel solution at a 1:1 vol ratio (v/v). This mixing was done carefully to ensure homogeneity, resulting in a final cell density of 1 × 10^7 cells/mL. 3 mL of the cell biomaterial mixture was drawn into a sterilized syringe with a 32 G

needle and set into the 3D printer at 11 °C. Each 3DP- HO was then fabricated by forced extrusion at a 150 mm3/min extrusion speed in a layer-by- layer fashion. The lobule-like hepatorganoids were later fully supplemented High Glucose Dulbecco's Modified Eagle Medium with 10 % Fetal Bovine Serum with a change of medium every 2 days, followed by biochemical analyses.

2.11. RNA sequencing and RT-qPCR

Total RNA was extracted according to the protocol of the RNA purification kit. For RNA sequencing, RNA samples were prepared and performed high-throughput sequencing at Tsingke Biotech Co., Ltd. RNA sequencing data had been approved and uploaded to GEO datasets of National Institute of Health (NIH, GSE269768; www.ncbi.nlm.nih.gov). Gene expression levels were quantified to facilitate data analysis. Bioinformatics analysis was performed to differentiate gene expression and explore gene ontology (GO), KEGG pathway enrichment and functional annotations. The results were visualized using tools available on the bioinformatics online platform. (https://www.bioinformatics.com.cn, last accessed on Apr 20, 2024).

For RT-qPCR, 1 μg of total RNA was used for cDNA synthesis using the RT-PCR kit. The qPCR process occurred employing the Applied Biosystems QuantStudio qPCR system (Thermo Fisher, USA). The β-actin expression served as an internal reference. The relative expression of the target genes was computed as $2^{-\Delta CT}$ (where $\Delta CT = \Delta CT^{\text{target gene}} - \Delta CT^{\beta\text{-actin}}$).

2.12. Immunofluorescence (IF)

The specimens were stabilized with 4 % paraformaldehyde (Sangon Biotech, China). Thereafter, 0.5 % Triton X-100 (Sigma, USA) was added, and the specimens were sealed with 5 % bovine serum albumin. Next, the specimens underwent incubation with diluted antibodies at 4 °C overnight. Following washing with PBST buffer, the specimens were incubated in fluoro-secondary antibodies at room temperature. After staining with DAPI (Beyotime, China), the specimens were examined using a fluorescence microscope.

2.13. Orthotopic implantation

4 week-age BALB/c nude mice were brought from Ziyang Experimental Animal TEC. Mice were anaesthetized by 2 % sodium pentobarbital. After anesthesia, median abdominal incision was made and left extrahepatic lobe was exposed. A 3-0 suture was pre-placed around the hepatic pedicle to temporally ligature the vessels in order to control bleeding. A lesion with 5 mm in diameter and 1 mm in depth was made and hepatorganoids was fixed on the lesion with tissue glue (3M Vetbond, Cat. 1469SB). After implantation and coagulation, the suture was removed and the incision was closed.

2.14. Hematoxylin and eosin (H&E) staining and immunohistochemistry (IHC) staining

Tissue samples was typically worked up into formalin-fixed paraffin-embedd (FFPE) sections. Cut tissue sections into thin slices of 5 mm thick. After deparaffinization and rehydration, slides were immersed in a hematoxylin solution for a few minutes. After rinse and differentiation, slides was submerged in eosin solution for a few minutes. After that, slides were passed through graded alcohols to deghydrate and cleared in xylene. After mounting and drying, slides were examinated under a light microscope.

For immunohistochemistry (IHC) staining, deparaffinized and rehydrated slides were merged in citrate buffer for antigen retrieval and immersed in hydrogen peroxide to block endogenous peroxidase. Then, slides were incubated with a primary antibody dilution (hCD31, mCD31) at 37 °C for 1 h. After that, the slides were incubated in a 2-step EnVision Detection System (PV-9000, ZSGB-BIO Inc, China) for 30 min. DAB was utilized for color development. Slides were visualized and analyzed under light microscope.

2.15. Statistical analyses

Statistical analyses were conducted utilizing SPSS Statistics (version 20, IBM, USA) and Graphpad Prism software (version 8, USA). Quantitative data were analyzed using Student's t-test and one-way ANOVA. Significance levels were denoted as follow: $p < 0.05$ (*), $p < 0.01$ (**), $p < 0.001$ (***) and $p < 0.0001$ (****).

3. Results

3.1. GelMA/NHS/VEGF materials characterization

To fabricate of 3D bioprinting hepatorganoids, we assessed the biocompatibility, degradation, and stress modulus of tissue engineering materials. Live/dead assay indicated similar cell viabilities of HUVEC and Huh7 cells in 2D and 3D culture (Fig. 2A). CCK8 assay demonstrated notable enhancement of HUVEC proliferation in 3D culture comparing to 2D culture, and no significant difference of Huh7 prolieration in 2D and 3D culture (Fig. 2B). Then, we tested the compression and stress module of GelMA hydrogels in different concentrations (Fig. 2C).

Previous studies have reported that GelMA-based bioinks typically require concentrations above 7 % to facilitate localized gelation and photocrosslinking [16]. However, these higher concentrations often result in constructs with excessive stiffness, which can adversely affect cell viability and activity [17]. Our preliminary experiments also revealed that a 2 % GelMA hydrogel was challenging to photo-crosslink effectively, further guiding our exploration of suitable concentration ranges. Given that the stiffness of liver matrix is approximately 1 kPa [18], we tested GelMA concentrations ranging from 4 % to 10 %. Through this investigation, we determined that a 4 % GelMA concentration was optimal for our purposes, consistent with that previously reported for GelMA physical gels used in extrusion-based 3D bioprinting [17]. This concentration provided an appropriate matrix stiffness that closely mimics the natural liver environment, thereby promoting enhanced cell survival and functionality. Additionally, the 4 % GelMA demonstrated excellent rheological properties that were well-suited to our bioprinting strategy. To induce vascularization, we synthesized a GelMA hydrogel with controlled VEGF release (GelMA/NHS/VEGF) and assessed its material properties. In vivo degradation studies showed similar degradation profiles for both GelMA/NHS/VEGF and GelMA (Fig. 2D and E). However, we compared the VEGF release kinetics of GelMA/NHS/VEGF and GelMA/VEGF, confirming the controlled release from GelMA/NHS/VEGF (Fig. 2F). This mechanism involves NHS reacting with amino groups on bioactive proteins, forming stable amide bonds, which facilitate the conjugation of target proteins with double-bond-modified polymers, enabling sustained release [19]. As depicted in Supplementary Fig. 1, Modification of bovine serum albumin (BSA) with AC-PEG(5K)-NHS increases its molecular weight from approximately 65 kDa by about 5 kDa, enhancing protein anchoring and modulating release kinetics.

Therefore, while *in vivo* degradation experiments indicate no significant differences in degradation rates between GelMA and GelMA/NHS/VEGF, in vitro studies demonstrate that the release rate of VEGF from GelMA/NHS/VEGF is significantly slower than that of the control group. This suggests that the controlled release is not solely dependent on degradation but is also significantly influenced by the chemical interactions facilitated by NHS, which enhance VEGF anchoring and modulate its release.

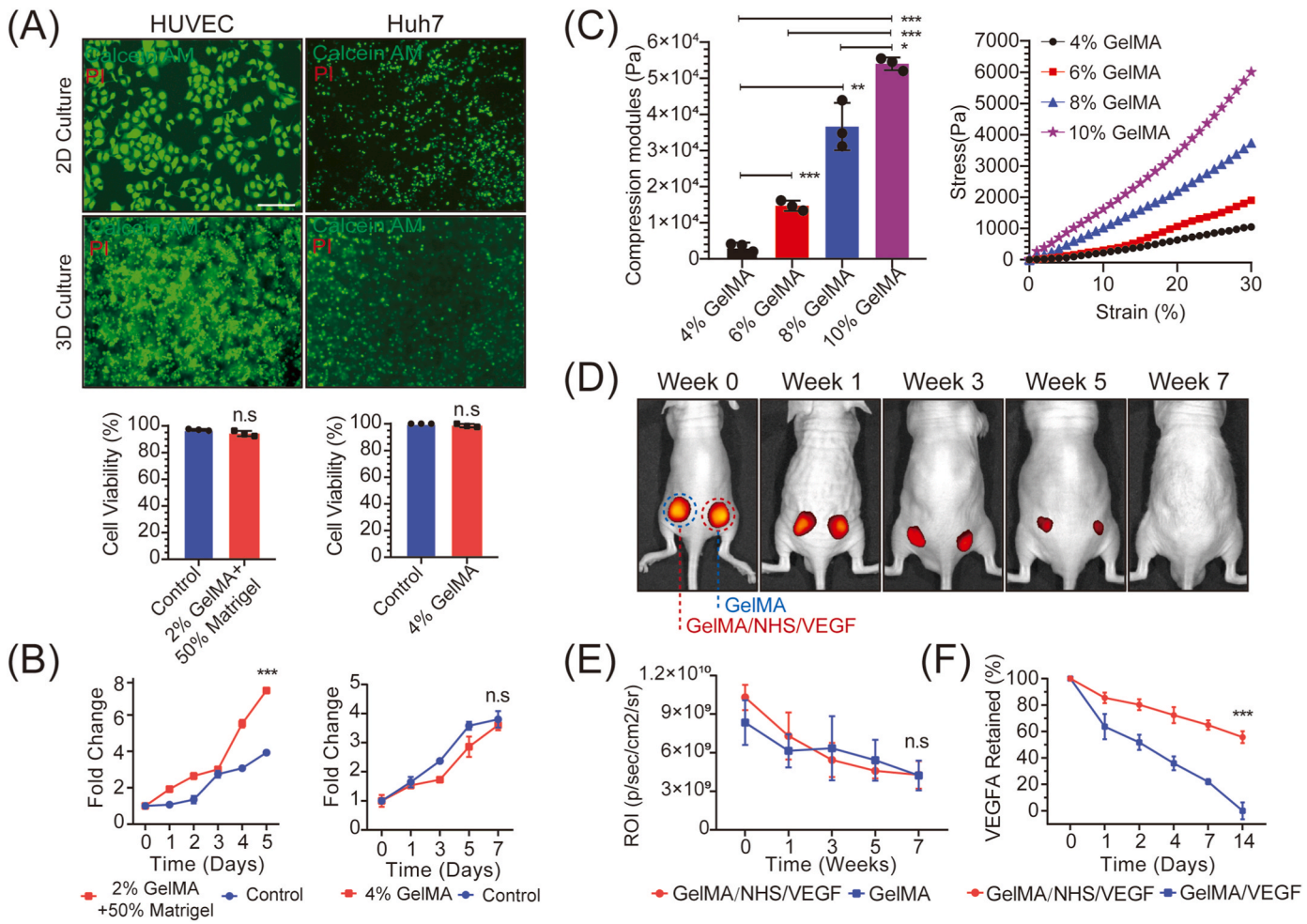

Fig. 2. Characterization of GelMA/NHS/VEGF hydrogel.
A. Live/dead assay of HUVEC and Huh7 cells in 2D and 3D culture. Scale bar: 200um.
B. CCK8 of HUVEC and Huh7 cells in 2D and 3D culture.
C. Compression module of GelMA hydrogels in different concentrations.
D. Degradation *in vivo* of GelMA/NHS/VEGF and GelMA hydrogel.
E. Measurement of degradation *in vivo* of GelMA/NHS/VEGF and GelMA hydrogel.
F. VEGF-releasing kinetics of GelMA/NHS/VEGF and GelMA/VEGF.

3.2. 3D bioprinting lobule-like hepatorganoids exhibited the highest viability in vivo and in situ

As aiming to implant engineered hepatorganoids *in situ*, we developed luciferase-expressing Huh7 cells, encapsulated cells in 4 % GelMA hydrogel and assessed this system in orthotopic implantation model (Supplementary Fig. 2A). Live imaging revealed vitality of hepatorganoids after implantation (Supplementary Figs. 2B and 2C). However, this vitality of hepatorganoids declined rapidly within 2 weeks (Supplementary Fig. 2B). Meanwhile, ALB concentration in serum exhibited a significant elevation following hepatorganoids orthotopic implantation compared to the control group (Supplementary Fig. 2D). Additionally, H&E staining demonstrated residual grafts infiltrating into native liver parenchyma at the implantation site periphery (Supplementary Fig. 2E).

Utilizing GFP-Huh7 and RFP-MSCV-293T cells, we verified the capacity and precision of 3D Bioplotter in accomplishing 3D bioprinting with complex structure and bioinks (Supplementary Fig. 3B). To determine the optimal geometric architecture for hepatorganoids, we devised and separately 3D bioprinting multiple architectures (loose 90°-crossed, dense 90°-crossed, 60°-crossed, control) of hepatorganoids with 3D Bioplotter (Supplementary Figs. 3C and 3D). However, the live/dead assay indicated diminished cell viability within the inner layers of hepatorganoids (Supplementary Figs. 3E and 3F), suggesting the necessity for an advanced geometric architecture for better viability. This observation highlights a potential limitation in the current design of the hepatorganoids, where insufficient nutrient and oxygen diffusion or waste removal in the inner regions may lead to compromised cell survival. Such findings underscore the importance of optimizing the geometric architecture of the hepatorganoids to enhance their structural and functional characteristics.

Subsequently, we originally designed and fabricated lobule-like hepatorganoids (Fig. 3A). The lobule-like structure of hepatorganoids were inspired by the natural architecture of liver lobules. Consistent with other reported studies [9,20,21], lobule-like design could overcome diffusion limitations and support cell viability throughout the construct. Evaluation of live/dead assay indicated robust viability across all sections of the lobule-like hepatorganoids (Fig. 3A). Furthermore, hypoxia assay demonstrated superior oxygen uptake by hepatocytes within the hepatorganoids compared to other architectures (Fig. 3B. Relative hypoxia fluorescence intensity, lobule vs. 60°, 90°, control, 0.4880 vs 1.009, 0.6778, 0.8704, $p < 0.01$. Relative hypoxia fluorescence area, lobule vs. 60°, 90°, control, 0.4005 vs 0.5663, 0.4985, 0.6159, $p < 0.05$.) The SEM image shows the highly porous

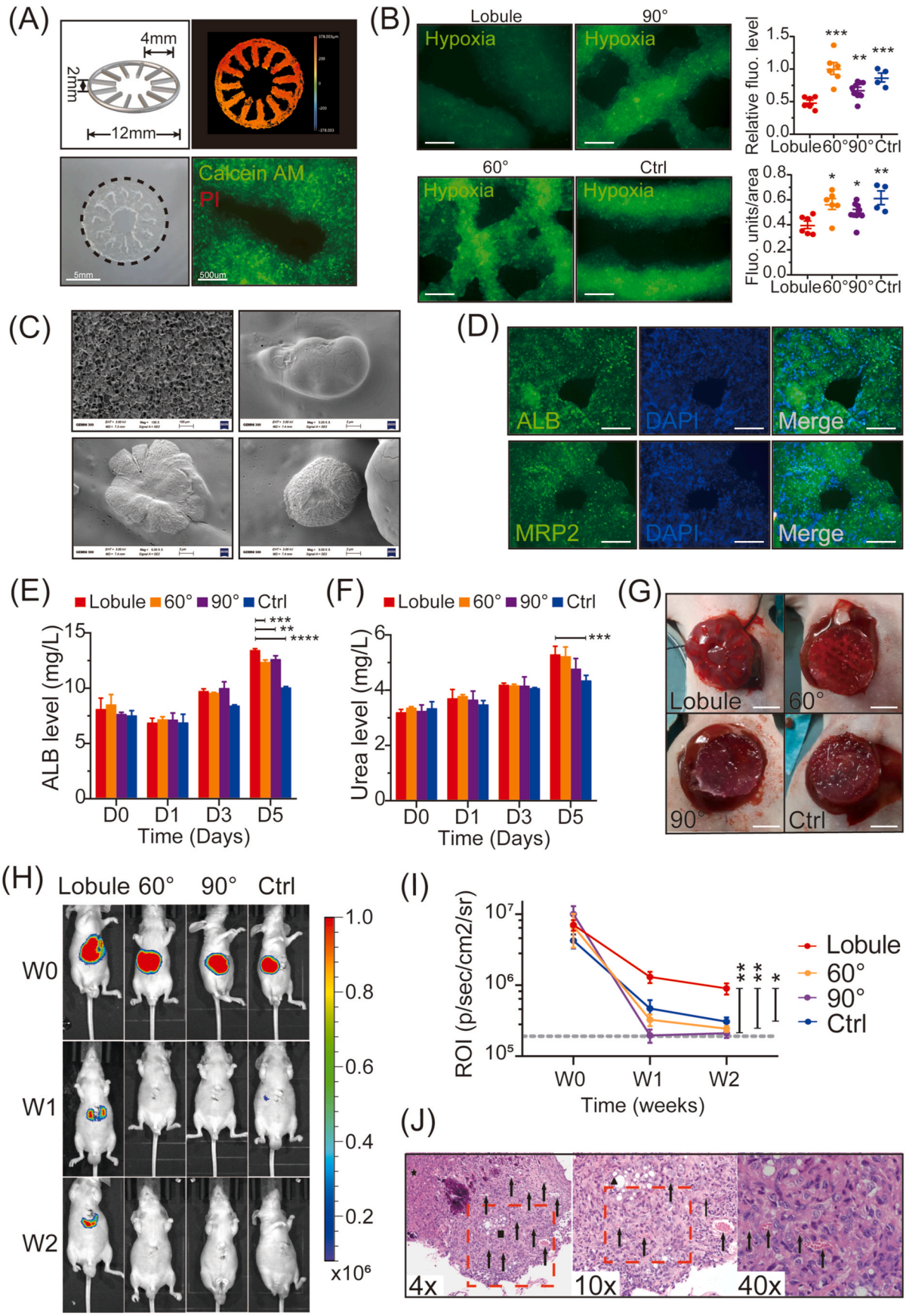

(caption on next page)

Fig. 3. Characterization of 3D bioprinting lobule-like hepatorganoids.
A. Fabrication of 3D bioprinting lobule-like hepatorganoids.
B. Hypoxia assay of hepatorganoids in different architetures. Scale bar: 500um.
C. Scanning electron microscopic images of hepatorganoids.
D. Immunofluorescence results of ALB and MRP2 in the lobule-like hepatorganoids. Scale bar: 500um.
E. ALB secretion in different architectural designs of hepatorganoids.
F. Urea nitrogen secretion in different architectural designs of hepatorganoids.
G. Orthotopic implantation of different architectural designs of hepatorganoids. Scale bar: 5 mm.
H. Live imaging *in situ* results of different architectural designs of hepatorganoids.
I. Live imaging *in situ* analyses of different architectural designs of hepatorganoids.
J. H&E staining of the lobule-like hepatorganoids following orthotopic implantation. (The asterisk represents normal liver tissue, the triangle indicates the newly formed blood vessels, and the square denotes the transplanted liver tissue.)

microstructure of the GelMA hydrogel. The interconnected porous network provides a conducive environment for cell proliferation and migration by facilitating nutrient and oxygen diffusion. This structural feature is critical for supporting cellular activities and mimicking the extracellular matrix (Fig. 3C). The magnified image illustrates hepatocytes with well-defined morphology embedded in the GelMA hydrogel. The porous nature of the hydrogel allows the cell to maintain its shape and interact with its microenvironment, further demonstrating the material's biocompatibility and suitability for tissue engineering applications. Immunofluorescence results highlighted the expression of crucial hepatic markers, ALB and MRP2, in the lobule-like hepatorganoids (Fig. 3D). Additionally, ALB secretion examination indicated significant higher production in the lobule-like hepatorganoids compared to other architectural designs (Fig. 3E lobule vs. 60°, 90°, control, 13.47 vs 12.39, 12.65, 10.08 mg/L, $p < 0.01$). Urea nitrogen assay demonstrated markedly increased urea production in the lobule-like hepatorganoids compared to the control group, while negligible differences observed compared to 60°-crossed and 90°-crossed groups (Fig. 3F lobule vs. 60°, 90°, control, 5.304 vs 5.233, 4.781, 4.358, $p < 0.01$). Afterwards, we conducted orthotopic implantation of lobule-like, 60°-crossed, 90°-crossed and control hepatorganoids (Fig. 3G). Live imaging indicated that lobule-like hepatorganoids persisted the highest viability *in situ* compared to other architectures (Fig. 3H and I). Furthermore, histological analysis demonstrated well-colonized grafts of lobule-like hepatorganoids within the native liver tissue. Besides, abundant angiogenesis was observed in

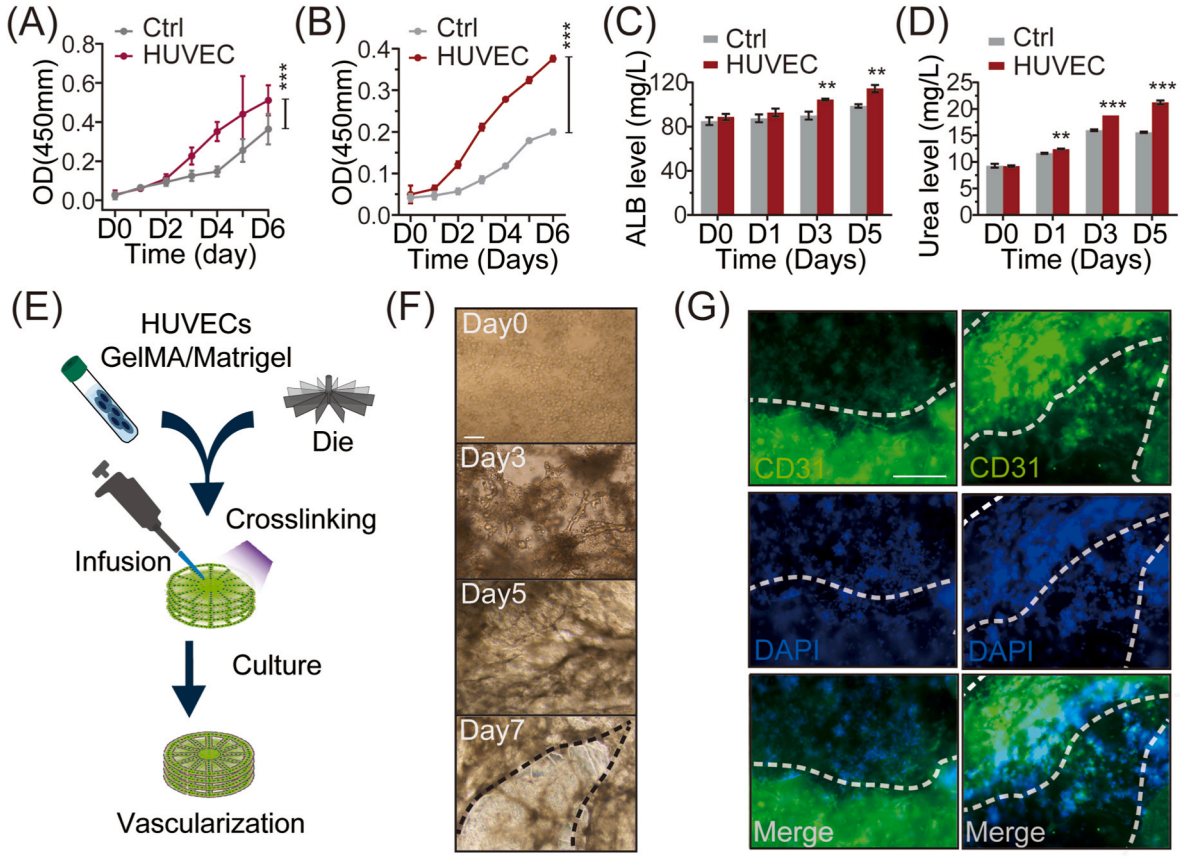

Fig. 4. HUVECs and GelMA/NHS/VEGF induced vascularization.
A. CCK8 assay of Huh7 proliferation cultured with the conditional medium from HUVECs.
B. CCK8 assay of Huh7 proliferation co-cultured with HUVECs.
C. ALB secretion in Huh7 co-cultured with HUVECs.
D. Urea nitrogen secretion in Huh7 co-cultured with HUVECs.
E. Scheme diagram of manufacturing vascularized lobule-like hepatorganoids.
F. Light microscopic images observing the process of self-assembly vascularization. Scale bar: 100um.
G. Immunofluorescence results of CD31 in the vascularized lobule-like hepatorganoids. Scale bar: 275um.

the grafts, providing sufficient blood and oxygen supply to the lobule-like hepatorganoids following orthotopic implantation (Fig. 3J).

3.3. HUVECs and GelMA/NHS/VEGF collaborative induced vascularization of 3D bioprinting lobule-like hepatorganoids

As HUVECs are commonly used in tissue engineering for supportive cell, we examined their impact on growth of hepatocytes. We gathered the culture medium from HUVECs and prepared the conditional medium by mixing it with fresh culture medium for Huh7 culture. The CCK8 assay indicated that conditional medium from HUVECs promoted Huh7 proliferation compared to control (0.5117 vs 0.3638, $p < 0.001$; Fig. 4A). Moreover, when HUVECs were co-cultured with Huh7, a significant increase in Huh7 proliferation was observed compared to the

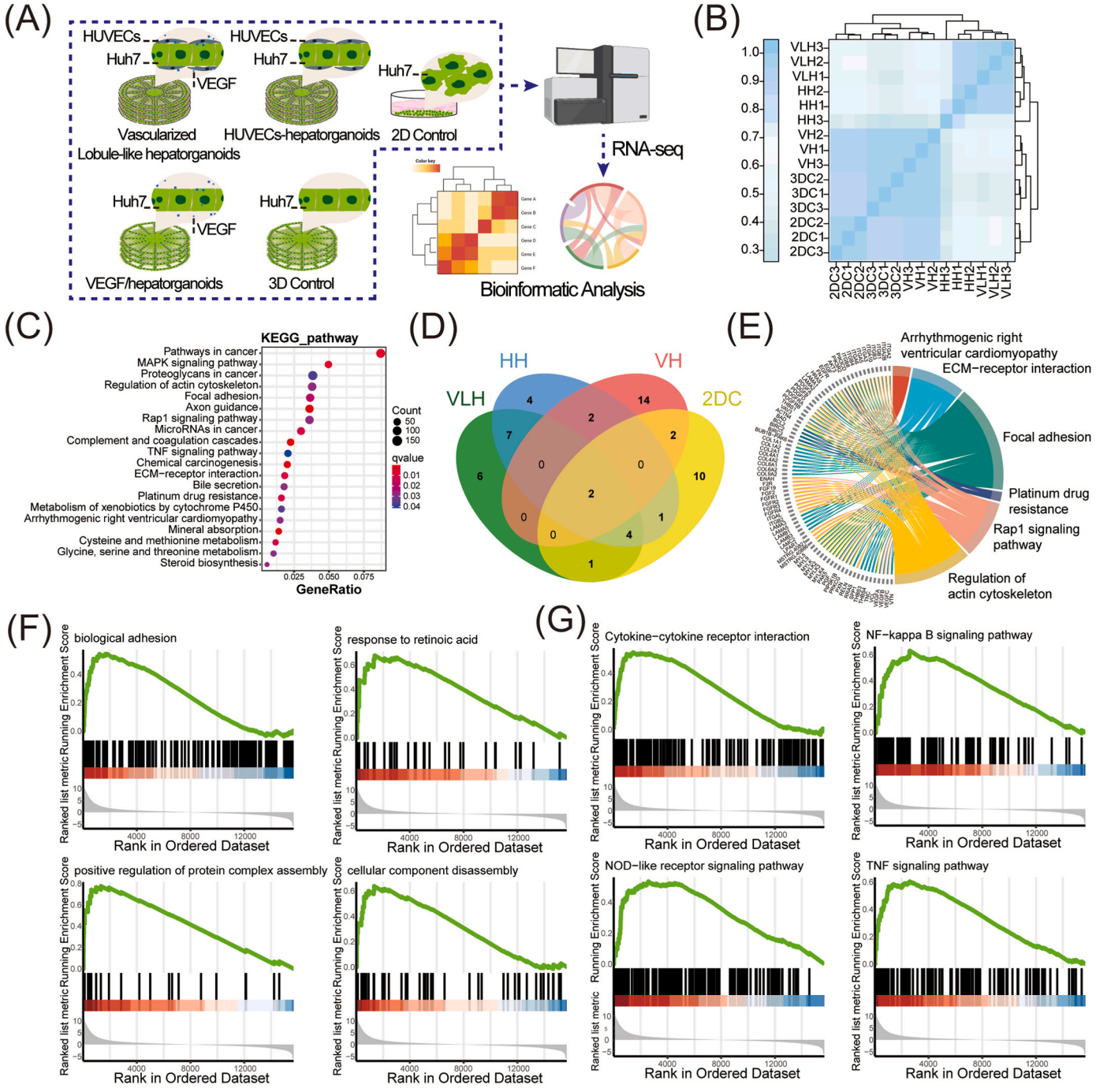

Fig. 5. Transcriptomics analysis of vascularized lobule-like hepatorganoids.
A. Scheme diagram of transcriptomics analysis of vascularized lobule-like hepatorganoids.
B. Correlation analysis of multiple groups of 3D bioprinting lobule-like hepatorganoids.
C. KEGG pathway analysis of vascularized lobule-like hepatorganoids.
D. Venn diagram of multiple groups of 3D bioprinting lobule-like hepatorganoids.
E. Cord diagrams of vascularized lobule-like hepatorganoids.
F. Biological processes of vascularized lobule-like hepatorganoids.
G. GESA analysis of vascularized lobule-like hepatorganoids.

control group (Supplementary Fig. 4). Subsequent CCK8 assays confirmed that Huh7 exhibited notably faster growth when co-cultured with HUVECs than the control group (0.3761 vs 0.1999, $p < 0.001$) (Fig. 4B). Meanwhile, examination of albumin and urea secretion indicated significant higher levels in the HUVEC-Huh7 co-culture group compared to the control group (114.4 vs 98.75 mg/L, $p < 0.01$; 21.24 vs 15.59 mg/L, $p < 0.001$. Fig. 4C and D).

Given the pronounced effect of HUVECs on promoting hepatocyte growth, we devised a method to create a bioink comprising HUVECs, 2 % GelMA/50 % Matrigel, which was then infused into the center of lobule and molded with a 3D-printing metal die (Fig. 4E, Supplementary Video 1). The selection of 50 % Matrigel was primarily based on its well-documented efficacy in angiogenesis assays. This concentration is commonly used to promote the tubulogenic of HUVECs, providing a supportive environment that mimics the extracellular matrix, thus facilitating the formation of vascular-like structures [22]. Incorporating 2 % GelMA into the mixture was inspired by the previous studies [23], where a GelMA-Matrigel microgel system was successfully employed to encapsulate lung cancer organoids.

By combining GelMA with Matrigel, we aimed to leverage the structural benefits of GelMA, such as its photocrosslinkable properties, alongside the biological activity of Matrigel. This hybrid bioink was designed to enhance the mechanical stability of the printed constructs while promoting the angiogenic potential of HUVECs. Continuous observation demonstrated a self-assembly process of HUVECs forming networks around lobule-like hepatorganoids, eventually leading to vascularization (Fig. 4F). Immunofluorescence analysis indicated the expression of the vascular marker CD31 on the surface and in the gaps between adjacent cords of lobule-like hepatorganoids (Fig. 4G).

3.4. Transcriptomics revealed the underlying mechanism for enhanced viability of vascularized lobule-like hepatorganoids

For exploration the underlying mechanism for enhanced viability of vascularized lobule-like hepatorganoids, we established several experimental groups: vascularized lobule-like hepatorganoids (VLH), HUVECs-hepatorganoids (HH), VEGF/hepatorganoids (VH), 3D control (3DC) and 2D control (2DC) groups. We subjected these groups to RNA sequencing and subsequent bioinformatics analysis (Fig. 5A). Correlation and cluster analysis indicated distinguished patterns among the groups, with VLH and HH groups showing remarkable gene expression patterns, while VH and 3DC exhibited distinct gene expression profiles (Fig. 5B and Supplementary Fig. 4A).

KEGG pathway analysis of VLH unveiled several up-regulated pathways, including focal adhesion, ECM-receptor interaction, regulation of actin cytoskeleton, bile secretion, Rap1 signaling pathway, and multiple amino acid metabolism pathways (Fig. 5C). Conversely, KEGG pathway analysis of VH and HH highlighted different sets of up-regulated pathways (Supplementary Figs. 4B and 4C). We then identified unique up-regulated pathways in VLH through Venn diagram analysis, indicating 6 pathways distinct to VLH (Fig. 5D). Further exploration via cord diagrams demonstrated that these pathways predominantly involved genes related to focal adhesion, regulation of actin cytoskeleton, ECM-receptor interaction and the Rap1 signaling pathway (Fig. 5E).

Additionally, Gene Set Enrichment Analysis (GSEA) uncovered biological processes and KEGG pathways specifically up-regulated in VLH, which included cell adhesion, proliferation, cell interaction and various metabolic processes (Fig. 5F and G). On the other side, GSEA analysis of VH and HH identified different sets of enriched processes, such as glycolysis, cell interaction, hypoxia in VH, and angiogenesis, cell adhesion, extracellular structure remodeling in HH separately (Supplementary Figs. 4D and 4E).

3.5. The activation of GAS6/AXL and LAMB3/ITGA3 signaling pathways in vascularized lobule-like hepatorganoids enhances angiogenesis and proliferation

Given the vigorous proliferation of hepatocytes within the context of hydrogel interaction in VLH, we investigated the crucial gene regulating cell regeneration and ECM receptor interaction. Through Gene Ontology (GO) analysis of cell regeneration (Fig. 6A) and KEGG pathway analysis of ECM receptor interaction (Fig. 6B), we noticed the up-regulation of the GAS6/AXL signaling pathway, recognized for its role in liver regeneration; and several laminin/integrin complexes in VLH.

Volcano diagram demonstrated GAS6/AXL and LAMB3/ITGA3 significantly up-regulated in VLH (Fig. 6C). RNA sequencing data confirmed a substantial elevation of GAS6/AXL and LAMB3/ITGA3 expression levels in VLH and HH (Fig. 6D). Moreover, RT-qPCR results demonstrated a marked increase in GAS6/AXL and LAMB3/ITGA3 expression in VLH compared to other groups (Fig. 6E).

Immunofluorescence staining results further validated the heightened expression of GAS6/AXL in VLH compared to control groups (Fig. 6F). In addition, LAMB3/ITGA3 expression levels were notably elevated in VLH compared to control groups (Fig. 6G).

3.6. Long-term viability maintenance of vascularized lobule-like hepatorganoids following orthotopic implantation

Subsequent to orthotopic implantation of VLH, HH, VH and 3DC hepatorganoids we sought to validate the maintenance of viability *in situ* post-implantation. Live imaging assessments revealed that VLH exhibited the most robust viability following orthotopic implantation compared to the HH, VH and 3DC groups (Fig. 7A). Moreover, the luciferin signal of the VLH group presented relative long-term consistency and growth throughout extended observation (Fig. 7B).

Serological marker α-fetoprotein (AFP) levels were significantly elevated in the VLH group compared to other groups (74588 vs 6497, 6646, 7689 ng/mL; $p < 0.05$. Fig. 7C). Following a 5weeks implantation period, mice were sacrificed, and grafts were harvested for comparison (Fig. 7D). Grafts from the VLH group exhibited significantly larger sizes compared to those from the HH, VH and 3DC groups (Fig. 7E), and the grafts-liver ratio in the VLH group was significantly larger than in the HH, VH and 3DC groups (Fig. 7F).

Furthermore, histological analysis was conducted to discern histological disparities among the groups. Grafts in the VLH and HH groups displayed markedly more abundant vasculogenesis compared to those in the VH and 3DC groups (Fig. 7G). Additionally, we sought to determine whether the vessels formed within the grafts originated from the transplanted HUVECs or were induced from the host. Immunohistochemistry analysis revealed that human-derived CD31 was negative on vasoendothelial cells within the grafts, while mouse-derived CD31 was positive, suggesting that the vessels within the grafts originated from host induction rather than the transplanted HUVECs (Fig. 7G).

4. Discussion

Hepatocytes are contact-dependent cells that rely on cell-cell and cell-matrix interactions within the hepatic tissue microenvironment to maintain their survival and phenotypes. In regular two-dimensional culture systems, primary hepatocytes often experience decreased proliferative capacity, rapid de-differentiation, and loss of liver-specific functions. However, tissue engineering biomaterials can provide a three-dimensional culture architecture that offers microenvironment for cell adhesion and growth, thereby enabling the long-term maintenance of specific physiologic properties [24], significantly enhancing proliferative capacity and biological activity, making suitable for creating artificial hepatorganoids and bioreactors [25]. Research on biomaterials mainly focus on optimizing biomaterials, improving environmental adaptability, enhancing cell loading efficiency, and promoting cell

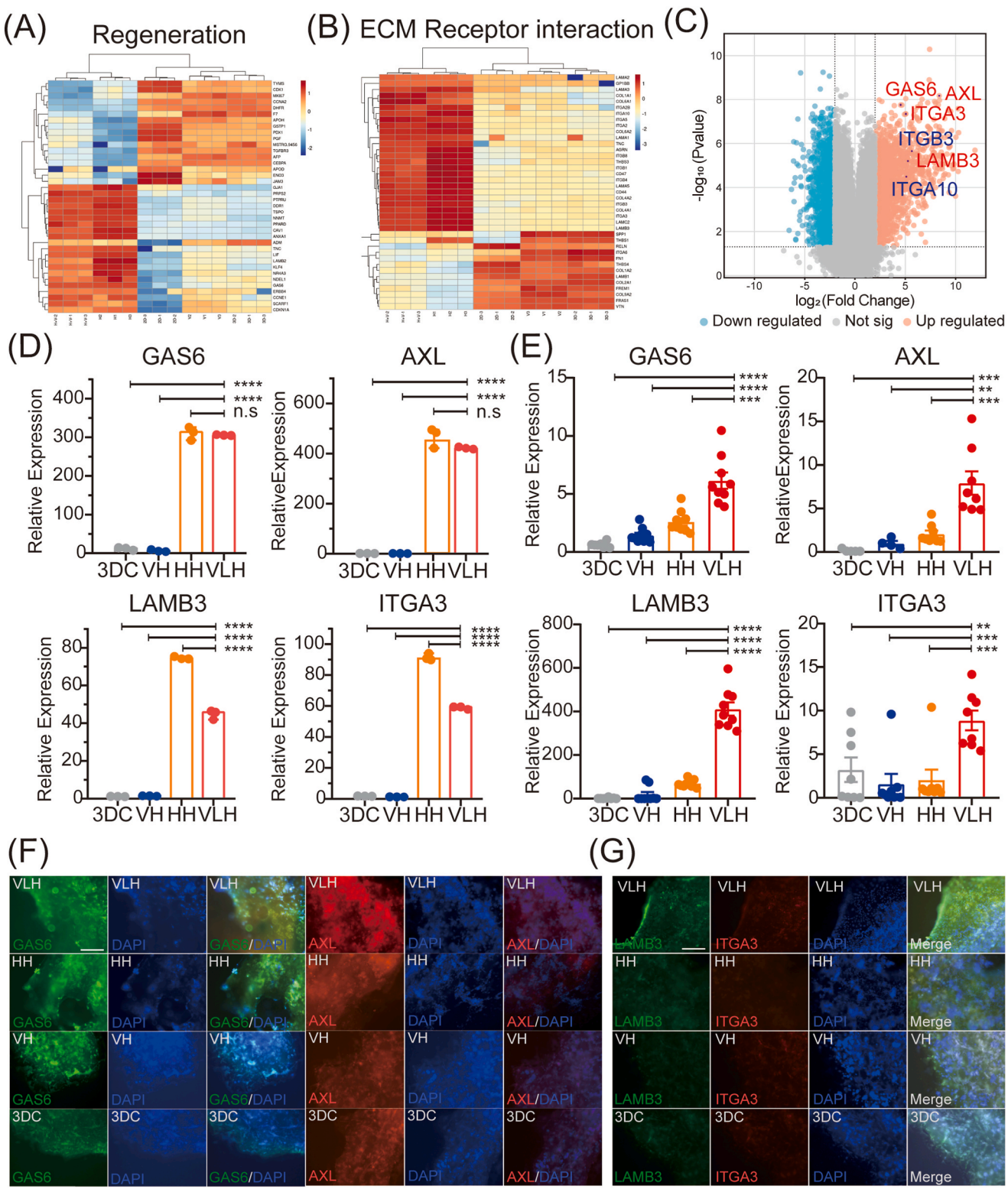

Fig. 6. GAS6/AXL and LAMB3/ITGA3 Signaling Pathways activated in vascularized lobule-like hepatorganoids.
A. GO analysis of cell regeneration in vascularized lobule-like hepatorganoids.
B. KEGG pathway analysis of ECM receptor interaction in vascularized lobule-like hepatorganoids.
C. Volcano diagram of gene expression alteration in vascularized lobule-like hepatorganoids.
D. RNA sequencing data of GAS6/AXL and LAMB3/ITGA3 expression levels in hepatorganoids.
E. RT-qPCR results of GAS/AXL and LAMB3/ITGA3 expression in hepatorganoids.
F. Immunofluorescence staining of GAS6/AXL in hepatorganoids. Scale bar: 275um.
G. Immunofluorescence staining of LAM3/ITGA3 in hepatorganoids. Scale bar: 275um.

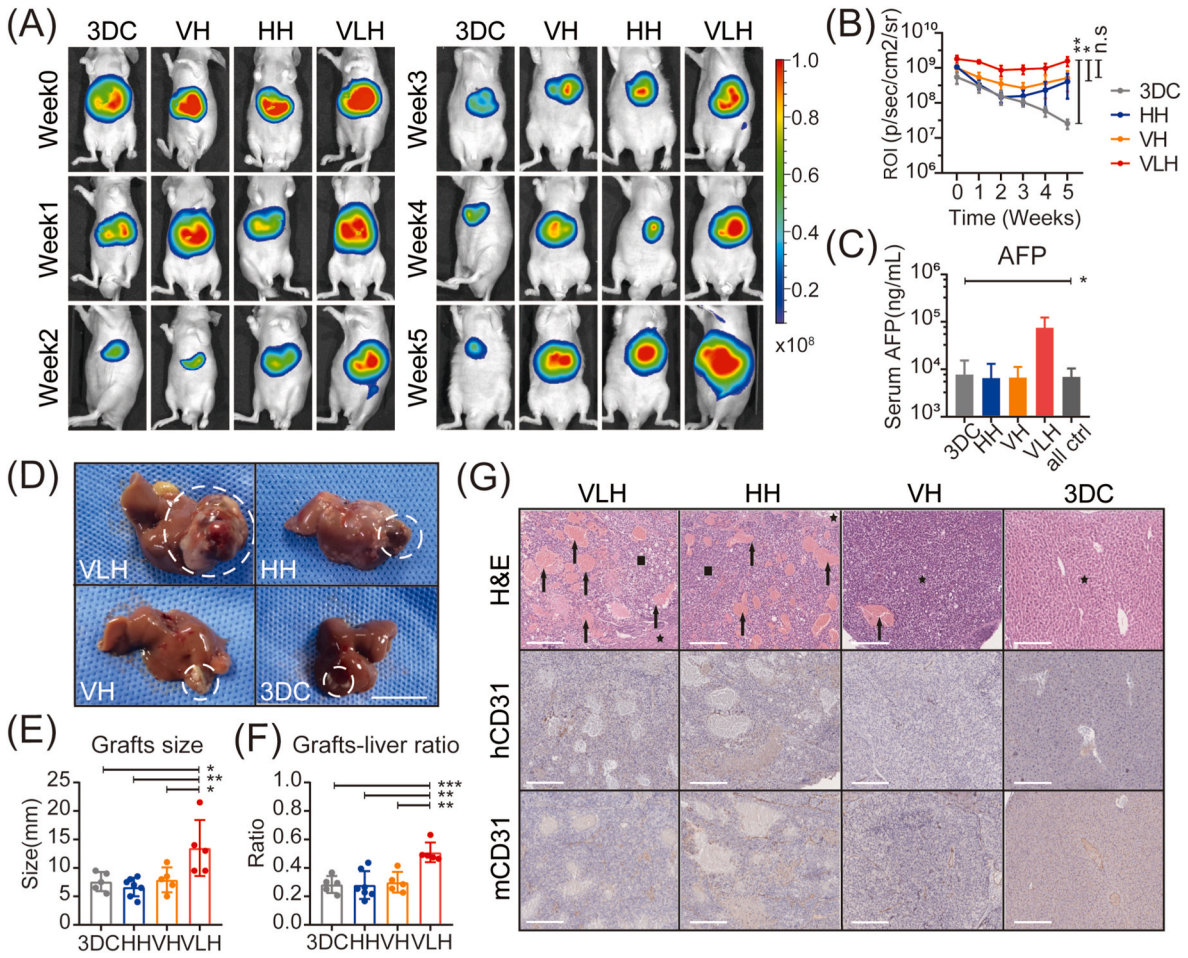

Fig. 7. Long-term viability maintenance of vascularized lobule-like hepatorganoids following orthotopic implantation.
A. Live imaging assessments of hepatorganoid viability *in situ* following orthotopic implantation.
B. Live imaging results of long-term consistency of hepatorganoids.
C. AFP levels of hepatorganoid viability*itu* following orthotopic implantation.
D. Specimen of hepatorganoid grafts following orthotopic implantation. Scale bar: 1 cm.
E. Size of hepatorganoid grafts following orthotopic implantation.
F. Grafts-liver ratios of hepatorganoid grafts following orthotopic implantation.
G. H&E and immunohistochemistrical analysis of grafts following orthotopic implantation. Scale bar: 250um. (The asterisk represents normal liver tissue, the triangle indicates the newly formed blood vessels, and the square denotes the transplanted liver tissue.)

functionality.

Vascularization of tissue-engineering hepatorganoids plays a crucial role in nutrition supplement, gas exchange, substance metabolism, and homeostasis maintenance. Studies have demonstrated that the diffusion distance of oxygen and nutrients is restricted in about 200 μm, which means that if the gap between cells and vascular network is above the limitation, it can lead to hypoxia and necrosis [26]. The liver is one of the most highly vascularized organs in body, with hepatocytes requiring a high amount of oxygen and nutrients, and having a lower tolerance for hypoxia and a low-nutrient environment. Therefore, establishing a vascularized system in tissue-engineering hepatorganoids is of utmost importance for long-term cultivation, maintenance of the cellular microenvironment, and preservation of functionality [6]. Wang et al. highlighted the potential of hydrogel composites to enhance vascularization through improved mechanical properties, printability, and angiogenic activities of HUVEC, providing a novel approach for hepatorganoids vascularization [27].

Currently, the studies focus lies in the improvement of the 3D bioprinting process on tissue-engineering vascularized hepatorganoids. Ma et al. presented a two-step digital light processing (DLP)-based 3D bioprinting system to construct triculture architecture embedding induced-hepatic progenitor cells with HUVEC and adipose-derived stem cells, and found improved morphology, liver-specific gene expressions and activities [18]. Janani et al. developed a vascularized lobule-like liver model with ECM-based bioink laden with hepatocyte-like cells (HLCs), HUVECs and stellate cells using an extrusion-based bioprinting approach, and demonstrated that the liver model facilitated the synthetic and metabolic activities [10]. Kang et al. utilized a preset extrusion bioprinting technique to manufacture multicellular (hepatic and endothelial cells) hepatic lobules simultaneously, and found an accelerated cellular organization with preserved vascularized integrity and enhanced cellular functions [28]. Gu et al. presented simultaneously assemble heterogeneous cells into hepatic functional units through an acoustic differential bioassembly technique based on different physical characteristics including size and buoyant density, and achieved organotypic models with spatially-defined architectures [29]. In addition, pre-vascularized liver hydrogel microspheres containing hepatocytes and vascular endothelial cells have been reported in the literature, with potential to be applied in granular bioprinting as a method to construct vascularized hepatorganoids. Deng et al. reported a hydrogel microsphere-encapsulated HLCs for self-assembled prevascularized liver tissue, showing improved hepatic morphology, marker expression,

functions and successful intrahepatic engraftment [30]. Hong et al. demonstrated a production of hepatic-lobule-like micro-tissue spheroids by a precursor cartridge and microfluidic emulsification incorporating bioprinting system. These multiple cell microtissue spheroids allowed long-term culture with ideal viability and structural integrity in vitro, and stable implantation *in vivo* [31]. Fang et at. Developed a granular cell aggregated-based biphasic bioink (GCAB) packing hepatic cell aggregates, and printed dense hepatic tissues with GCAB and an endothelial cell-laden bioink, showing improved vascularization and metabolic functions [32].

Indeed, there is still a significant gap to achieve the goal of vascularized tissue-engineering hepatorganoids for orthotopic implantation. Despite the advancements in 3D bioprinting techniques, creating fully functional and vascularized hepatorganoids that can be implanted on liver remains complex challenges, mainly due to the following reasons. Firstly, the current level of biomanufacturing at the millimeter level of precision, which is unable to accomplish micro-capillary networks at the micrometer level. Secondly, the functional and inductive materials for vascularization requires further optimization. Simply using hydrogel materials to load growth factors results in a relatively rapid release within a short time after manufacture, making it difficult to sustain the promotion of cell activity and blood vessel formation. Moreover, the critical molecular mechanisms and gene expressions that promote vascularization in tissue engineering hepatorganoids are still unclear.

In order to overcome these challenges, we suggested a 3D bioprinting lobule-like hepatorganoids with induced vascularization by spontaneous self-assembling capillary networks of vascular endothelial cells on the constructs. Compared to 2D culture, vascular endothelial cells and hepatocytes maintained viability in 3D culture. According to stiffness of liver matrix, we tested the mechanical modules of different GelMA and identified 4 % GelMA with the most similarity of liver matrix. Based on the results, we optimized a hydrogel delivery system based on GelMA with stable degradation and controlled-releasing vascular endothelial growth factor (VEGF). Constructed by utilizing an N-hydroxysuccinimide (NHS) modified dual-functional polyethylene glycol (PEG) cross-linker (AC-PEG-NHS) to anchor VEGF, the GelMA/NHS/VEGF hydrogel could achieve VEGF controlled-release after orthotopic implantation compared to GelMA/VEGF without AC-PEG-NHS, allowing for sustained and stable induction of angiogenesis. Then, we created a lobule-like shape of hepatorganoids, and employed a 3D bioprinting approach to accomplish the architecture. This lobule-like hepatorganoids, which predefine the path for endothelial cells to facilitating the self-assembled capillary network formation, contained higher priority of oxygen supply, albumin and urea secretion in vitro and viability maintenance and angiogenesis *in vivo* than other architectures. We infused HUVECs embedded by 2 % GelMA/50 % Matrigel into lobule-like hepatorganoids, which were then developed into vascularized lobule-like hepatorganoids (VLH) with self-assembled caplillary network. This self-assembled capillary network could remarkably enhance substance exchange and nutrient metabolism, and it promotes orthotopic implantation and vascular regeneration. Furthermore, using omics techniques and bioinformatics analysis, we performed analyses on RNA sequencing data of hepatocytes in tissue engineering hepatorganoids. These analyses helped uncover molecular signaling pathways associated with organoid cultivation and vascularization. We found upregulation in GAS6/AXL and LAMB3/ITGA3 signaling pathways, which are involved in angiogenesis and proliferation, providing inspiration for fabrication of a precisely regulated vascularized lobule-like hepatorganoids. VLHs significantly improved and maintained hepatocytes viability and functionality following orthotopic implantation, and we delved into the key molecular mechanisms behind the formation of vascularization and the maintenance of functional activity in VLHs. Eventually, VLHs suggested the longest viability and the most abundant angiogenesis in liver post-orthotopic implantation.

Our study still has some limitations. First, we primarily addressed the question of vascularization and long-term survival of engineered hepatorganoids after orthotopic implantation. However, there is still a long distance to go in finding an ideal strategy to achieve specific hepatic functions in orthotopic-implanted hepatorganoids, such as bile synthesis and metabolism. Second, we conducted the orthotopic implantation in BALB/c nude mice, which are a strain with impaired immunity. There remains a challenge of orthotopic hepatorganoids implantation in hosts with intact immunity to avoid immune reactions. Furthermore, the implantation of exogenous sources of cells and organoids continues to face ethical and safety problems. Further investigations are required to improve the design and production of hepatorganoids for orthotopic implantation to address these limitations.

5. Conclusion

This research will provide an innovative and highly effective construction of 3D bioprinting lobule-like hepatorganoids with induced vascularization for orthotopic implantation. It aims to uncover the mechanisms that promote vascularization and maintain functional activity, ultimately offering a promising and effective new strategy for the treatment of various acute and chronic liver injuries, as well as insufficient residual liver function following major liver resections in clinical practice.

CRediT authorship contribution statement

Jianing Yan: Writing – original draft, Visualization, Investigation, Funding acquisition, Formal analysis, Data curation, Conceptualization. **Zhichao Ye:** Writing – original draft, Visualization, Formal analysis, Data curation. **Yiwei Lu:** Writing – original draft, Visualization, Formal analysis, Data curation. **Yuyang Yuan:** Formal analysis, Data curation. **Xiaofeng Wang:** Formal analysis, Data curation. **Tingting Yan:** Formal analysis, Data curation. **Jun Yin:** Writing – review & editing, Conceptualization. **Yifan Wang:** Writing – review & editing, Funding acquisition, Conceptualization.

Ethical approval

This study was approved by the Laboratory Animal Welfare and Ethics Review of Zhejiang University (NO. ZJU20240448).

Sources of funding

This study was supported by National Natural Science Foundation of China (Grant No.82170616), Major Program of Natural Science Foundation of Zhejiang Province, China (Grant No.LHDMD23H030001), East China Pharmaceutical Joint Funds of Natural Science Foundation of Zhejiang Province, China (Grant No.LHDMY23H070008), and General Program of Natural Science Foundation of Zhejiang Province, China (Grant No. LQ24H030007).

Declaration of competing interest

The authors declare no conflict of interest.

Appendix A. Supplementary data

Supplementary data to this article can be found online at https://doi.org/10.1016/j.mtbio.2025.101515.

Data availability

Data will be made available on request.

References

[1] H. Reinke, G. Asher, Circadian clock control of liver metabolic functions, Gastroenterology 150 (3) (2016) 574–580.
[2] P. Kubes, C. Jenne, Immune responses in the liver, Annu. Rev. Immunol. 36 (2018) 247–277.
[3] N. Jalan-Sakrikar, T. Brevini, R.C. Huebert, et al., Organoids and regenerative hepatology, Hepatology 77 (1) (2023) 305–322.
[4] H. Yang, L. Sun, Y. Pang, et al., Three-dimensional bioprinted hepatorganoids prolong survival of mice with liver failure, Gut 70 (3) (2021) 567–574.
[5] D.H. Kim, M.J. Kim, S.Y. Kwak, et al., Bioengineered liver crosslinked with nano-graphene oxide enables efficient liver regeneration via MMP suppression and immunomodulation, Nat. Commun. 14 (1) (2023) 801.
[6] W. Lv, H. Zhou, A. Aazmi, et al., Constructing biomimetic liver models through biomaterials and vasculature engineering, Regenerative biomaterials 9 (2022) rbac079.
[7] X. Liu, X. Wang, L. Zhang, et al., 3D liver tissue model with branched vascular networks by multimaterial bioprinting, Adv. Healthcare Mater. 10 (23) (2021) e2101405.
[8] H. Lee, S. Chae, J.Y. Kim, et al., Cell-printed 3D liver-on-a-chip possessing a liver microenvironment and biliary system, Biofabrication 11 (2) (2019) 025001.
[9] D. Kang, G. Hong, S. An, et al., Bioprinting of multiscaled hepatic lobules within a highly vascularized construct, Small 16 (13) (2020).
[10] G. Janani, S. Priya, S. Dey, et al., Mimicking native liver lobule microarchitecture in vitro with parenchymal and non-parenchymal cells using 3D bioprinting for drug toxicity and drug screening applications, ACS applied materials & interfaces 14 (8) (2022) 10167–10186.
[11] A. Enrico, D. Voulgaris, R. Östmans, et al., 3D microvascularized tissue models by laser-based cavitation molding of collagen, Advanced materials (Deerfield Beach, Fla) 34 (11) (2022) e2109823.
[12] A. Grosso, A. Lunger, M.G. Burger, et al., VEGF dose controls the coupling of angiogenesis and osteogenesis in engineered bone, NPJ Regen. Med. 8 (1) (2023) 15.
[13] D. Lu, K. Cai, Z. Zeng, et al., VEGF loading heparinized hyaluronic acid macroporous hydrogels for enhanced 3D endothelial cell migration and vascularization, Biomater. Adv. 167 (2025) 214094.
[14] M.G. Burger, A. Grosso, P.S. Briquez, et al., Robust coupling of angiogenesis and osteogenesis by VEGF-decorated matrices for bone regeneration, Acta Biomater. 149 (2022) 111–125.
[15] E. Quinlan, A. LóPEZ-Noriega, E.M. Thompson, et al., Controlled release of vascular endothelial growth factor from spray-dried alginate microparticles in collagen-hydroxyapatite scaffolds for promoting vascularization and bone repair, Journal of tissue engineering and regenerative medicine 11 (4) (2017) 1097–1109.
[16] L.E. Bertassoni, J.C. Cardoso, V. Manoharan, et al., Direct-write bioprinting of cell-laden methacrylated gelatin hydrogels, Biofabrication 6 (2) (2014).
[17] W.J. Liu, M.A. Heinrich, Y.X. Zhou, et al., Extrusion bioprinting of shear-thinning gelatin methacryloyl bioinks, Adv. Healthcare Mater. 6 (12) (2017).
[18] X. Ma, X. Qu, W. Zhu, et al., Deterministically patterned biomimetic human iPSC-derived hepatic model via rapid 3D bioprinting, Proc. Natl. Acad. Sci. U.S.A. 113 (8) (2016) 2206–2211.
[19] J.C. Sun, X.Y. Xie, Y.Y. Song, et al., Selenomethionine in gelatin methacryloyl hydrogels: modulating ferroptosis to attenuate skin aging, Bioact. Mater. 35 (2024) 495–516.
[20] Q.J. Mao, Y.F. Wang, Y. Li, et al., Fabrication of liver microtissue with liver decellularized extracellular matrix (dECM) bioink by digital light processing (DLP) bioprinting, Mater. Sci. Eng., C (2020) 109.
[21] Z.C. Fan, X.Y. Wei, K.K. Chen, et al., 3D bioprinting of an endothelialized liver lobule-like construct as a tumor-scale drug screening platform, Micromachines 14 (4) (2023).
[22] M.G. Fois, Z.N.T. Birgani, C. Lopez-Iglesias, et al., In vitro vascularization of 3D cell aggregates in microwells with integrated vascular beds, Materials Today Bio 29 (2024).
[23] Y.M. Zhang, Q.F. Hu, Y.Q. Pei, et al., A patient-specific lung cancer assembloid model with heterogeneous tumor microenvironments, Nat. Commun. 15 (1) (2024).
[24] Y. Wang, C.T. Nicolas, H.S. Chen, et al., Recent advances in decellularization and recellularization for tissue-engineered liver grafts, Cells Tissues Organs 204 (3–4) (2017) 125–136.
[25] N. Prior, P. Inacio, M. Huch, Liver organoids: from basic research to therapeutic applications, Gut 68 (12) (2019) 2228–2237.
[26] A. Aazmi, H. Zhou, W. Lv, et al., Vascularizing the brain in vitro, iScience 25 (4) (2022) 104110.
[27] X. Wang, X. Liu, W. Liu, et al., 3D bioprinting microgels to construct implantable vascular tissue, Cell Prolif. 56 (5) (2023) e13456.
[28] H.J. Cho, H.J. Kim, K. Lee, et al., Bioengineered multicellular liver microtissues for modeling advanced hepatic fibrosis driven through non-alcoholic fatty liver disease, Small 17 (14) (2021) e2007425.
[29] L.J. Gu, S.Q. Jiang, X.D. Xu, et al., Size- and density-dependent acoustic differential bioassembly of spatially-defined heterocellular architecture, Biofabrication 15 (1) (2023).
[30] S. Deng, X. Zhao, Y. Zhu, et al., Efficient hepatic differentiation of hydrogel microsphere-encapsulated human pluripotent stem cells for engineering prevascularized liver tissue, Biofabrication 15 (1) (2022).
[31] G. Hong, J. Kim, H. Oh, et al., Production of multiple cell-laden microtissue spheroids with a biomimetic hepatic-lobule-like structure, Advanced materials (Deerfield Beach, Fla) 33 (36) (2021) e2102624.
[32] Y. Fang, M. Ji, Y. Yang, et al., 3D printing of vascularized hepatic tissues with a high cell density and heterogeneous microenvironment, Biofabrication 15 (4) (2023).